RSC Advances

PAPER

View Article Online
View Journal | View Issue



Cite this: *RSC Adv.*, 2019, **9**, 32833

# Segregation-free bromine-doped perovskite solar cells for IoT applications†

Itaru Raifuku,[ab] Yasuaki Ishikawa,[*a] Yu-Hsien Chiang,[b] Pei-Ying Lin,[b] Ming-Hsien Li,[b] Yukiharu Uraoka[a] and Peter Chen[b]

Received 12th July 2019
Accepted 10th October 2019

DOI: 10.1039/c9ra05323a

rsc.li/rsc-advances

Perovskite solar cells have attracted much attention as next-generation solar cells because of their high efficiency and low fabrication costs. Moreover, perovskite solar cells are a promising candidate for indoor energy harvesting. We investigated the effect of bandgap tuning on the characteristics of triple cation-based perovskite solar cells under fluorescent lamp illumination. According to the current density–voltage curves, perovskite solar cells with a wider bandgap than the conventional one exhibited improved open-circuit voltage without sacrificing short-circuit current density under fluorescent lamp illumination. Moreover, the wider bandgap perovskite films including a large amount of bromine in the composition did not show phase segregation, which can degrade the photovoltaic performance of perovskite solar cells, after fluorescent lamp illumination. Our results demonstrate the facile strategy to improve the performance of perovskite solar cells under ambient lighting and great potential of perovskite solar cells for indoor applications such as power sources for the internet of things.



## Introduction

Perovskite solar cells (PSCs), in which perovskite-structured materials ($APbX_3$, A: organic cation, X: halogen) act as the light absorbing layer, have recently attracted much attention because of their solution processability and extremely high power conversion efficiency (PCE).[1,2] Miyasaka *et al.* first reported PSCs with a PCE of 3.8% in 2009; in their study, the device structure was similar to that of liquid dye-sensitized solar cells.[3] In 2012, Snaith *et al.* developed solid-state PSCs by replacing the electrolyte with an organic semiconductor.[4] After that, many approaches to improve the PCE have been attempted, such as optimizing the fabrication process, controlling the composition of the perovskite materials, adding additives, and applying interface modification.[5–22] To date, a maximum PCE of 23.3%, which is comparable to those of crystalline silicon and semiconductor compound solar cells, has been reported.[23] Since high-temperature annealing is necessary to form the mesoporous $TiO_2$ layer for PSCs, rigid glass is mainly used as the substrate. However, low-temperature processes have also been investigated, and flexible PSCs have been reported; therefore, many PSC applications, such as installation on curved spaces, are expected.[24–26] The main issues in their commercialization are their stability and the presence of Pb, which is toxic, but several approaches have already been applied to overcome these problems. For example, Pb-free PSCs based on Sn, Bi, Sb, and Ti have been tested; they exhibited a potential to boost the PCE,[27–33] although its value was lower than that of Pb-based ones, and part of them showed enormous stability.[30,33] This enables us to expect the commercialization of PSCs.

Since PSCs consist of an n-type electron transport layer (ETL), a perovskite layer, and a p-type hole transport layer (HTL), their device structure is a type of p-i-n junction; in such a structure, the internal electrical field controls the carrier transport, and the carrier recombination is inhibited even under low-level injection conditions. In addition, perovskite materials have defect tolerance, that is, fewer defect states are formed within their bandgap,[34] and this property could reduce recombination and allow high voltage. Because of these properties, PSCs can work efficiently even under low-illuminance conditions; in fact, our previous study demonstrated that they can maintain a high open-circuit voltage ($V_{OC}$) under a 0.1 mW $cm^{-2}$ illumination.[35] Compared with amorphous silicon solar cells which have also p-i-n structure, PSCs have shown lower $V_{OC}$ loss and higher $V_{OC}$ values under low-illuminance conditions. Furthermore, several groups reported that PSCs can perform under ambient lightings, such as a fluorescent lamp or light emitting diode (LED) illumination.[36–40] Brown *et al.* demonstrated that PSCs show PCE of 25.0% and 26.9% under 200 lx and 400 lx LED illumination, respectively.[40] In addition, they found flexible PSCs module can also perform under such low-illuminance conditions.[36] These reports suggest that PSCs can pave the road to the next generation of indoor energy harvesting devices.

[a]*Division of Materials Science, Nara Institute of Science and Technology, 8916-5 Takayama, Ikoma, Nara 630-0192, Japan. E-mail: yishikawa@ms.naist.jp*

[b]*Department of Photonics and Hierarchical Green-Energy Materials (Hi-GEM) Research Center, National Cheng Kung University, No.1, University Rd., Tainan, 701, Taiwan*

† Electronic supplementary information (ESI) available. See DOI: 10.1039/c9ra05323a

$CH_3NH_3PbI_{3-x}Cl_x$, which have a band gap of around 1.55 eV, was used as the light absorber of PSCs in the above reports. Although the bandgap is a suitable value for solar cells under sunlight, the value is bit small for indoor applications.[41] In this work, we investigated the effect of bandgap tuning on the performance of PSCs under low-illuminance conditions. We found that wide-bandgap Br-rich PSCs show better photovoltaic performance than the conventional one under fluorescent lamp illumination. Particularly, Br-rich PSCs showed higher $V_{OC}$ (forward scan: 0.803 V, reverse scan: 0.815 V) than the conventional PSCs (forward scan: 0.685 V, reverse scan: 0.778 V) under fluorescent lamp illumination (200 lx, 65 μW $cm^{-2}$). It is known that PSCs employing Br-rich perovskite materials show phase segregation which leads poor photovoltaic performance under common condition such as 1 sun irradiation. However, our results indicated that the phase segregation does not occur under ambient lighting. Bandgap tuning by controlling the Br ratio of perovskite materials is available in not only lead halide perovskite but also lead-free perovskite materials. Therefore, our findings provide beneficial strategy to apply PSCs for indoor energy harvesting, which can be implemented for future development of internet of things (IoT) applications.

## Experimental

### Fabrication of perovskite solar cells

Glass substrates (8 Ohm per sq, Pilkington TEC8) coated with fluorine-doped tin oxide (FTO) were etched using zinc powder and HCl (2 M) and then rinsed with pure water, ethanol, and acetone. To prepare the ETL, titanium diisopropoxide bis(acetylacetonate) (75 wt% in isopropanol, Sigma-Aldrich) diluted in ethanol (1 : 39, volume ratio) was sprayed on the FTO-coated substrates at 475 °C. Next, the substrates were annealed at 475 °C for 30 min. A mesoporous $TiO_2$ layer was deposited on the ETL by spin-coating a $TiO_2$ paste (30 NR-D, GreatCell Solar Co.) diluted in ethanol (1 : 8, weight ratio) at 4000 rpm for 30 s, and successively, the substrates were annealed at 500 °C for 30 min. A perovskite layer was deposited by spin-coating on the mesoporous $TiO_2$ in a two-step process: first, the substrates were accelerated to 2000 rpm for 10 s (200 rpm $s^{-1}$) and then spun at 5000 rpm for 20 s (2000 rpm $s^{-1}$), and second, chlorobenzene (200 μL) was dropped onto the rotating substrate for 5 s before the end of the spin-coating process. The compositions of the precursor solutions are shown in Table S1.† After spin-coating, the substrates were annealed at 100 °C for 1 h. Then, a solution of 2,2′,7,7′-tetrakis(*N*,*N*′-di-*p*-methoxyphenylamine)-9,9′-spirobifluorene (17 mg) of 4-*tert*-butylpyridine (6.9 μL) and lithium bis(trifluoromethanesulfonyl)imide (4.2 μL, 520 mg $mL^{-1}$ in acetonitrile) in chlorobenzene (240 μL) was spin-coated on the perovskite layer at 4000 rpm for 30 s to deposit an HTL. Finally, an Au electrode was deposited by thermal evaporation on the HTL.

### Characterization

The current density–voltage (*J*–*V*) characteristics were measured under air mass 1.5 global (AM1.5G) illumination (1 sun, 100 mW $cm^{-2}$) using a solar simulator (SS-F5 3A, Enlitech), calibrated using a reference silicon solar cell (SRC2000, Enlitech), and a source meter (2401, Keithley). The low-illuminance characteristics were measured under T5 fluorescent lamp illumination (200 lx, 65 μW $cm^{-2}$) with another source meter (2420, Keithley). The emission spectrum of the fluorescent lamp used is shown in Fig. S1.† The emission spectrum and intensity of the fluorescent lamp was measured using Sun Spectroradiometer (S-2440, Soma optics). The active area of the samples was set as 0.16 $cm^2$. The external quantum efficiency (EQE) was determined with an EQE measurement system (Newport Cornerstone 260). The X-ray diffraction (XRD) measurements were measured with D8 ADVANCE ECO (Bruker). The photoluminescence (PL) measurements were carried out by using a diode laser with 532 nm light source (intensity: 127 mW). The absorption spectra of the perovskite films were measured with an ultraviolet/visible light/near-infrared spectrophotometer (JASCO, V-570).

## Results and discussion

Two compositions of cesium containing triple cation-based perovskite materials, $Cs_{0.05}FA_{0.79}MA_{0.16}Pb(I_{0.84}Br_{0.16})_3$ (3-cat-Br16) and $Cs_{0.05}FA_{0.79}MA_{0.16}Pb(I_{0.50}Br_{0.50})_3$ (3-cat-Br50) (FA = formamidinium, MA = methylammonium), were used as the light absorbers in the tested PSCs. Increasing the Br content allows the bandgap increase in perovskite materials.[42] Fig. 1(a) shows the absorption spectra of both compounds; 3-cat-Br16 and 3-cat-Br50 exhibited absorption edges of 780 and 680 nm, respectively. Fig. 1(b) shows XRD patterns of both perovskite films. Three signature diffraction peaks of perovskite films were appeared at around 14°, 29°, and 32° which corresponding to (110), (220), and (310) planes. The diffraction peaks of 3-cat-Br50 films slightly shifted toward higher angle (Fig. S2†),

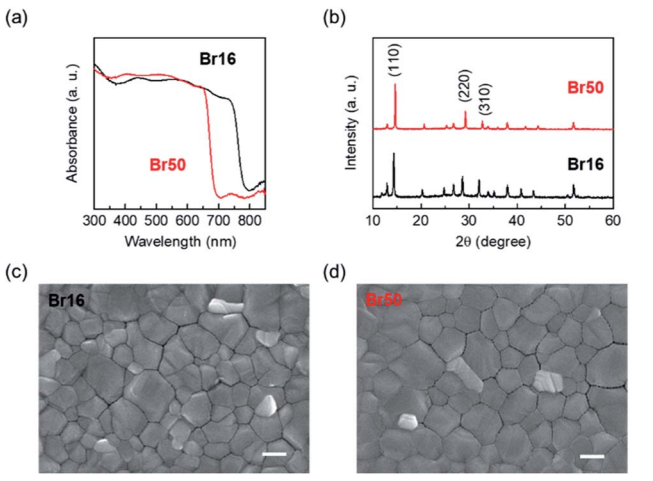


Fig. 1 (a) UV/vis spectra of $Cs_{0.05}FA_{0.79}MA_{0.16}Pb(I_{0.84}Br_{0.16})_3$ (3-cat-Br16) and $Cs_{0.05}FA_{0.79}MA_{0.16}Pb(I_{0.50}Br_{0.50})_3$ (3-cat-Br50) (FA = formamidinium, MA = methylammonium) perovskite films. The black and red lines represent absorbance spectra of 3-cat-Br16 and 3-cat-Br50 films, respectively. (b) XRD patterns of 3-cat-Br16 and 3-cat-Br50 films fabricated on FTO/$TiO_2$ substrates. (c) and (d) SEM images of 3-cat-Br16 and 3-cat-Br50 perovskite films. The scale bar is 200 nm.

indicating it has smaller lattice than 3-cat-Br16 films. Fig. 1(c) and (d) shows SEM images of both perovskite films. There was no significant difference in their morphology, which can affect their photovoltaic performance.

To evaluate the effect of bromine contents of perovskite films on the carrier lifetime, time-resolved photoluminescence (TRPL) measurement was carried out for both perovskite films. Fig. S3† shows TRPL spectrum of a 3-cat-Br16 film. The 3-cat-Br16 film showed fast decay ($\tau_1$) and slower decay ($\tau_2$) of 5.41 and 33.43 ns, respectively.

Fig. S4(b)† shows steady state PL spectra of 3-cat-Br50 films. The PL spectra were gradually changed during laser irradiation. This phenomenon might be attributed to phase segregation of bromine rich perovskite films discussed later. TRPL measurements of 3-cat-Br50 films were carried out with different detection wavelength of 676, 739, and 770 nm, that were observed as peaks and shoulders in steady state PL spectra. Fig. S4(a)† shows TRPL spectra of 3-cat-Br50 films. 3-cat-Br50 films showed different decay curves depending on detection wavelength. Further discussion is needed to determine the actual lifetime of bromine rich perovskite films. The lifetime of 3-cat-Br50 films calculated from TRPL spectra were summarized in Table S2.†

Fig. 2(a) shows the structure of the tested PSCs in this work. Fig. 2(b) displays the *J–V* curves of the 3-cat-Br16 PSCs measured under AM1.5G illumination (1 sun, 100 mW cm$^{-2}$), in forward and reverse scan; the highest PCE was 15.8% with a short-circuit current density ($J_{SC}$) of 20.99 mA cm$^{-2}$, a $V_{OC}$ of 1.033 V, and a fill factor (FF) of 0.730 in reverse scan (scan direction: from positive to negative bias). In forward scan (scan direction: from negative to positive bias), the highest PCE was 12.2% with a $J_{SC}$ of 20.72 mA cm$^{-2}$, a $V_{OC}$ of 0.964 V, and a FF of 0.612. Fig. 2(c) shows the *J–V* curves of the 3-cat-Br50 PSCs under the same condition. The highest PCE was 9.9% with a $J_{SC}$ of 15.19 mA cm$^{-2}$, a $V_{OC}$ of 1.026 V, a FF of 0.634, and 8.0% with a $J_{SC}$ of 15.27 mA cm$^{-2}$, a $V_{OC}$ of 0.952 V, a FF of 0.551 in reverse and forward scan, respectively. *J–V* characteristics of both PSCs were summarized in Tables S3 and S4.†

Fig. 2(d) shows the EQE spectra of both 3-cat-Br16 and 3-cat-Br50 PSCs, which exhibited EQE responses extended respectively to ~780 and ~680 nm, consistently with the absorption spectra of the corresponding perovskite films (Fig. 1(a)); both PSCs showed similar EQE values within their absorption regions. Although solar cells consisted with wide bandgap materials show high $V_{OC}$, they show low $J_{SC}$ value due to AM 1.5G spectrum with abundant long wavelength component. This is the reason why 3-cat-Br50 PSCs showed poor $J_{SC}$ and PCE than 3-cat-Br16 one under AM 1.5G irradiation. On the other hand, such long wavelength component is not included in common ambient lighting such as fluorescent lamp or LED (please see Fig. S1† for the spectrum). The absorption of 3-cat-Br50 PSCs (Fig. 1(a)) overlaps well with the fluorescent lamp (below 700 nm). Therefore, the results of EQE measurements enable us to expect that 3-cat-Br50 PSCs would show improved $V_{OC}$ without sacrificing $J_{SC}$ under fluorescent lamp illumination.

Fig. 2(e) and (f) displays the *J–V* curves of the 3-cat-Br16 and 3-cat-Br50 PSCs measured under fluorescent lamp illumination (200 lx, 65 μW cm$^{-2}$), respectively. In 3-cat-Br16 PSCs, $V_{OC}$ of

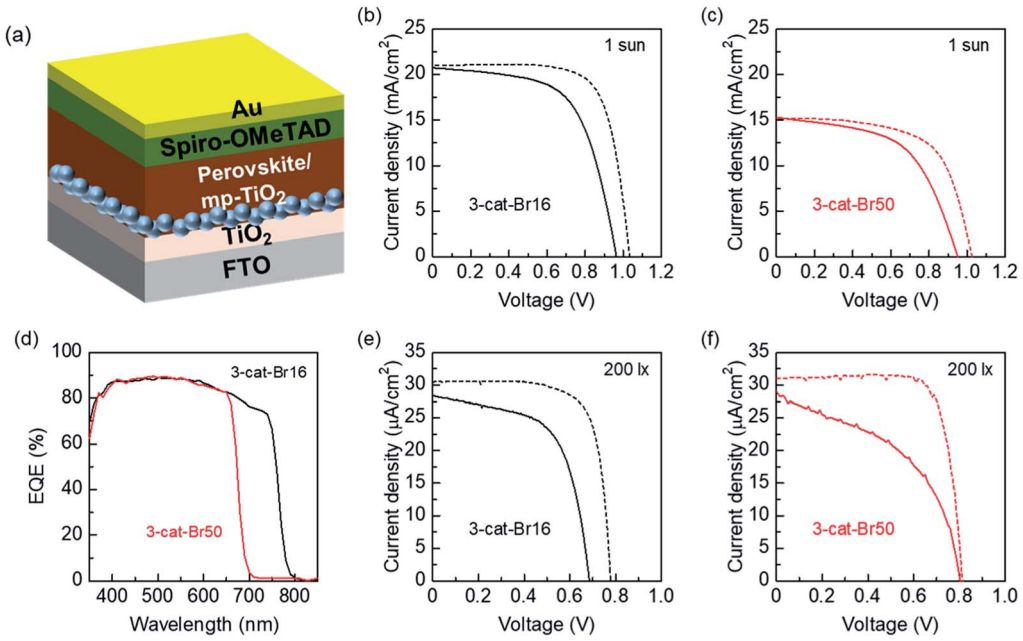


Fig. 2 (a) The schematic structure of perovskite solar cells (PSCs). (b) and (c) current density–voltage (*J–V*) curves of PSCs, having (b) $Cs_{0.05}FA_{0.79}MA_{0.16}Pb(I_{0.84}Br_{0.16})_3$ (3-cat-Br16) and (c) $Cs_{0.05}FA_{0.79}MA_{0.16}Pb(I_{0.50}Br_{0.50})_3$ (3-cat-Br50) (FA = formamidinium, MA = methylammonium) as light absorber, measured under AM 1.5 G (1 sun, 100 mW cm$^{-2}$) illumination. The solid and dashed lines represent the data from forward and reverse scan, respectively. (d) External quantum efficiency (EQE) spectra of PSCs. The black and red lines represent EQE spectra of 3-cat-Br16 and 3-cat-Br50 PSCs, respectively. (e) snd (f) *J–V* curves of (e) 3-cat-Br16 and (f) 3-cat-Br50 PSCs measured under fluorescent lamp illumination (200 lx, 65 μW cm$^{-2}$). The solid and dashed lines represent the data from forward and reverse scan, respectively.

0.685 and 0.778 V was observed in forward and reverse scan, respectively. On the other hand, 3-cat-Br50 PSCs showed $V_{OC}$ of 0.803 and 0.815 V in forward and reverse scan, respectively. The *J–V* characteristics were summarized in Tables S5 and S6.† As expected, 3-cat-Br50 PSCs showed improved $V_{OC}$ without sacrificing $J_{SC}$, leading to higher output.

Tables S5 and S6† also display PCE and maximum power output ($P_{MAX}$) calculated from *J–V* curves. Under fluorescent lamp illumination, 3-cat-Br50 PSCs showed $P_{MAX}$ of 11.0 and 19.7 μW $cm^{-2}$ which corresponds to PCE of 16.9% and 30.3% in forward and reverse scan, respectively. In case of our illumination condition, the light spectrum is quite a difference with the AM 1.5G. Freunek *et al.* reported the PCE of the absorber having 1.8 eV bandgap exceeds 40% in the case of fluorescent lamp,[41] suggesting our record of PCE over 30% is a possible value to achieve. However, our devices show large hysteresis, which makes it difficult to determine accurate PCE, indicating further investigations are needed to discuss the PCE. The PCE of PSCs under ambient lighting reported are summarized in Table S7†

As mentioned above, solar cells consisting of wide-bandgap materials commonly exhibit higher $V_{OC}$ than those made of narrow-bandgap. However, 3-cat-Br50 and 3-cat-Br16 PSCs showed similar $V_{OC}$ under AM1.5 G illumination. This phenomenon could be attributed to the phase segregation of mixed-halide perovskite materials, which has been reported in case of light irradiation[43–45] and results in the separation between iodine- and bromide-rich regions in the perovskite layer so that the iodine-rich region serves as charge recombination site to reduce the device $V_{OC}$ and FF. On the other hand, another study reported that this phase segregation takes a longer time under dark conditions[46] and occurs slower under low-illuminance condition than under AM1.5G illumination. Hence, this phase segregation might have not progressed during our measurements, leading to the higher $V_{OC}$ and FF of 3-cat-Br50 PSCs under low-illuminance conditions. In fact, the 3-cat-Br50 perovskite films exhibited a photoluminescence peak shift after the AM1.5 G 1 sun illumination for 45 min, as shown in Fig. 3(a). Fig. S5† shows PL shift of 3-cat-Br50 films with short time intervals. The PL shift started within 5 min during AM1.5G 1 sun irradiation. On the other hand, 3-cat-Br16 films did not show the PL shift after AM1.5G 1 sun illumination as shown in Fig. S6.† This tendency is consistent with previous reports on the phase segregation in mixed-halide perovskite films, but there are no studies on this phenomenon under the low-illuminance condition. We checked the phase segregation phenomenon under low-illuminance condition for 3-cat-Br50 films. Our experimental results explicitly exhibited no PL shift after the exposure of fluorescent lamp illumination (0.7 mW $cm^{-2}$ for 7 h) as shown in Fig. 3(b). These results suggested us that heavily bromine-doped perovskite solar cell opens the door of PSCs with bromide-rich active layer to use in indoor applications owing to its segregation-free phenomenon.

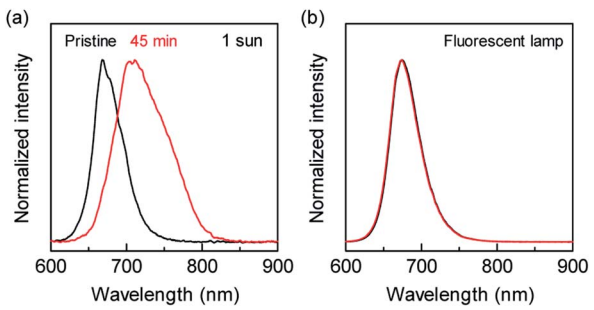


Fig. 3 Photoluminescence (PL) spectra of $Cs_{0.05}FA_{0.79}MA_{0.16}Pb(I_{0.50}Br_{0.50})_3$ (FA = formamidinium, MA = methylammonium) films exposed to (a) AM 1.5G and (b) fluorescent lamp illumination. The black and red lines represent PL spectra of before and after light soaking, respectively.

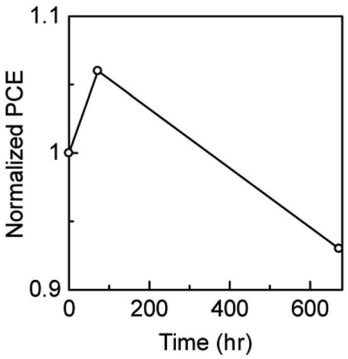


Fig. 4 Normalized power conversion efficiency (PCE) of sealed perovskite solar cells having $Cs_{0.05}FA_{0.79}MA_{0.16}Pb(I_{0.84}Br_{0.16})_3$ (FA = formamidinium, MA = methylammonium) as light absorber, stored under ambient condition.

We investigated the stability which is one of the crucial issues of PSCs for commercialization. 3-cat-Br16 PSC was used as the sample to neglect the influence of phase segregation. Fig. 4 shows the normalized PCE of the sealed PSCs after storage under ambient conditions, at room temperature, and in the dark. The sealing was carried out by fixing a glass cover on the PSCs using UV curing resin. The PSCs retained 93% of their initial efficiency after being stored under ambient condition (relative humidity ~35%) at room temperature and dark for 672 h. After 72 h, the PCE increased with increasing $V_{OC}$ and FF and then decreased with all the other parameters. The changes in the parameters and *J–V* curves before and after storage are shown in Fig. S7 and S8,† respectively. This result suggested that PSCs can operate long-term under indoor conditions, although heavily bromine-doped PSCs should also be examined in term of stability which is future work.

## Conclusions

We investigated the effect of bandgap tuning on the photovoltaic performance of triple-cation PSCs. Under AM1.5G 1 sun illumination, 3-cat-Br50 PSCs, which has an absorption edge of 680 nm, showed poor photovoltaic performance due to spectrum mismatch and phase segregation than conventional 3-cat-Br16 PSCs. By contrast, 3-cat-Br50 PSCs showed improved $V_{OC}$ without sacrificing $J_{SC}$, leading to higher power output than 3-cat-Br16 PSCs. We found that no-phase segregation occurred in

 

heavily bromine-doped PSC after the exposure of fluorescent lamp irradiation. In the stability test, sealed PSCs exhibited 93% of the initial PCE even after being stored for 672 h under ambient conditions, which indicates that there are no crucial stability issues for indoor applications. Our results demonstrate the facile strategy to improve the performance of PSCs under ambient lighting and great potential of PSCs for indoor applications such as dispersed power sources for the IoT.

## Conflicts of interest

There are no conflicts to declare.

## Acknowledgements

I. R. would like to thank Sachiko Morioka for the assistance with fabricating samples and Juan Paolo S. Bermundo for proofreading the manuscript. P. C. thanks the financial support from the Ministry of Science and Technology (106-2119-M-006 -004, 107-2221-E-006 -190-MY3). This work was financially supported by the Hierarchical Green-Energy Materials (Hi-GEM) Research Center, from the Featured Areas Research Center Program within the framework of the Higher Education Sprout Project by the Ministry of Education (MOE) in Taiwan.

## References

1 W. S. Yang, B.-W. Park, E. H. Jung, N. J. Jeon, Y. C. Kim, D. U. Lee, S. S. Shin, J. Seo, E. K. Kim, J. H. Noh and S. I. Seok, *Science*, 2017, **356**, 1376.
2 M. Saliba, T. Matsui, J.-Y. Seo, K. Domanski, J.-P. Correa-B, M. K. Nazeeruddin, S. M. Zakeeruddin, W. Tress, A. Abate, A. Hagfeldt and M. Grätzel, *Energy Environ. Sci.*, 2016, **9**, 1989.
3 A. Kojima, K. Teshima, Y. Shirai and T. Miyasaka, *J. Am. Chem. Soc.*, 2009, **131**, 6050.
4 M. M. Lee, J. Teuscher, T. Miyasaka, T. N. Murakami and H. J. Snaith, *Science*, 2012, **338**, 643.
5 J. Burschka, N. Pellet, S.-J. Moon, R. Humphry-Baker, P. Gao, M. K. Nazeeruddin and M. Grätzel, *Nature*, 2013, **499**, 316.
6 N. Ahn, D.-Y. Son, I.-H. Jang, S. M. Kang, M. Choi and N.-G. Park, *J. Am. Chem. Soc.*, 2015, **137**, 8696.
7 N. J. Jeon, J. H. Noh, Y. C. Kim, W. S. Yang, S. Ryu and S. I. Seok, *Nat. Mater.*, 2014, **13**, 897.
8 M. Xiao, F. Huang, W. Huang, Y. Dkhissi, Y. Zhu, J. Etheridge, A. Gray-Weale, U. Bach, Y.-B. Cheng and L. Spiccia, *Angew. Chem.*, 2014, **126**, 10056.
9 Y. Zhou, M. Yang, W. Wu, A. L. Vasiliev, K. Zhu and N. P. Padture, *J. Mater. Chem. A*, 2015, **3**, 8178.
10 M. Liu, M. B. Johnston and H. J. Snaith, *Nature*, 2013, **501**, 395.
11 C.-W. Chen, H.-W. Kang, S.-Y. Hsiao, P.-F. Yang, K.-M. Chiang and H.-W. Lin, *Adv. Mater.*, 2016, **26**, 6647.
12 N. J. Jeon, H. H. Noh, W. S. Yang, Y. C. Kim, S. Ryu, J. Seo and S. I. Seok, *Nature*, 2015, **517**, 476.
13 Y. Sun, J. Peng, Y. Chen, Y. Yao and Z. Liang, *Sci. Rep.*, 2017, **7**, 46193.
14 M. Zhang, J. S. Yun, Q. Ma, J. Zheng, C. F. J. Lau, X. Deng, J. Kim, D. Kim, J. Seidel, M. A. Green, S. Huang and A. W. Y. Ho-Baillie, *ACS Energy Lett.*, 2017, **2**, 438.
15 Z. Tang, T. Bessho, F. Awai, T. Kinoshita, M. M. Maitani, R. Jono, T. Murakami, H. Wang, T. Kubo, S. Uchida and H. Segawa, *Sci. Rep.*, 2017, **7**, 12183.
16 W. S. Yang, J. H. Noh, N. J. Jeon, Y. C. Kim, S. Ryu, J. Seo and S. I. Seok, *Science*, 2015, **348**, 1234.
17 P. Wang, J. Zhang, R. Chen, Z. Zeng, X. Huang, L. Wang, J. Xu, Z. Hu and Y. Zhu, *Electrochim. Acta*, 2017, **227**, 180.
18 Y. Zhao, J. Wei, H. Li, Y. Yan, W. Zhou, D. Yu and Q. Zhao, *Nat. Commun.*, 2016, **7**, 10228.
19 H. Lee, A. Kim, H.-C. Kwon, W. Yang, Y. Oh, D. Lee and J. Moon, *ACS Appl. Mater. Interfaces*, 2016, **8**, 29419.
20 Y. Wu, F. Xie, H. Chen, X. Yang, H. Su, M. Cai, Z. Zhou, T. Noda and L. Han, *Adv. Mater.*, 2017, **29**, 1701073.
21 L. Zuo, Z. Gu, T. Ye, W. Fu, G. Wu, H. Li and H. Chen, *J. Am. Chem. Soc.*, 2015, **137**, 2674.
22 H. Zhou, Q. Chen, G. Li, S. Luo, T. Song, H.-S. Duan, Z. Hong, J. You, Y. Liu and Y. Yang, *Science*, 2014, **345**, 542.
23 Q. Jiang, Y. Zhao, X. Zhang, X. Yang, Y. Chen, Z. Chu, Q. Ye, X. Li, Z. Yin and J. You, *Nat. Photonics*, 2019, **13**, 460.
24 A. Kogo, Y. Sanehira, Y. Numata, M. Ikegami and T. Miyasaka, *ACS Appl. Mater. Interfaces*, 2018, **10**, 2224.
25 J. Feng, X. Zhu, Z. Yang, X. Zhang, J. Niu, Z. Wang, S. Zuo, S. Priya, S. Liu and D. Yang, *Adv. Mater.*, 2018, **30**, 1801418.
26 B. Dou, E. M. Miller, J. A. Christians, E. M. Sanehira, T. R. Klein, F. S. Barnes, S. E. Shaheen, S. M. Garner, S. Ghosh, A. Mallick, D. Basak and M. F. A. M. van Hest, *J. Phys. Chem. Lett.*, 2017, **8**, 4960.
27 F. Gao, C. Li, L. Qin, L. Zhu, X. Huang, H. Liu, L. Liang, Y. Hou, Z. Lou, Y. Hu and F. Teng, *RSC Adv.*, 2018, **8**, 14025.
28 F. Hao, C. C. Stoumpos, D. H. Cao, R. P. H. Chang and M. G. Kanatzidis, *Nat. Photonics*, 2014, **8**, 489.
29 N. Ito, M. A. Kamarudin, D. Hirotani, Y. Zhang, Q. Shen, Y. Ogomi, S. Iikubo, T. Minemoto, K. Yoshino and S. Hayase, *J. Phys. Chem. Lett.*, 2018, **9**, 1682.
30 Z. Zhang, X. Li, X. Xia, Z. Wang, Z. Huang, B. Lei and Y. Gao, *J. Phys. Chem. Lett.*, 2017, **8**, 4300.
31 A. K. Baranwal, H. Masutani, H. Sugita, H. Kanda, S. Kanaya, N. Shibayama, Y. Sanehira, M. Ikegami, Y. Numata, K. Yamada, T. Miyasaka, T. Umeyama, H. Imahori and S. Ito, *Nano Convergence*, 2017, **4**, 26.
32 P. Karuppuswamy, K. M. Boopathi, A. Mohapatra, H.-C. Chen, K.-T. Wong, P.-C. Wang and C.-W. Chu, *Nano Energy*, 2018, **45**, 330.
33 M. Chen, M.-G. Ju, A. D. Carl, Y. Zong, R. L. Grimm, J. Gu, X. C. Zeng, Y. Zhou and N. P. Padture, *Joule*, 2018, **2**, 558.
34 K. X. Steirer, P. Schulz, G. Teeter, V. Stevanovic, M. Yang, K. Zhu and J. J. Berry, *ACS Energy Lett.*, 2016, **1**, 360.
35 I. Raifuku, Y. Ishikawa, S. Ito and Y. Uraoka, *J. Phys. Chem. C*, 2016, **120**, 18986.
36 G. Lucarelli, F. D. Giacomo, V. Zardetto, M. Creatore and T. M. Brown, *Nano Res.*, 2017, **10**, 2130.
37 J. Dagar, S. Castro-Hermosa, M. Gasbarri, A. L. Palma, L. Cina, F. Matteocci, E. Calabrò, A. D. Carlo and T. M. Brown, *Nano Res.*, 2018, **11**, 2669.

38 C.-Y. Chen, J.-H. Chang, K.-M. Chiang, H.-L. Lin, S.-Y. Hsiao and H.-W. Lin, *Adv. Funct. Mater.*, 2015, **25**, 7064.
39 F. D. Giacomo, V. Zardetto, G. Lucarelli, L. Cina, A. D. Carlo, M. Creatore and T. M. Brown, *Nano Energy*, 2016, **30**, 460.
40 J. Dagar, S. Castro-Hermosa, G. Lucarelli, F. Cacialli and T. M. Brown, *Nano Energy*, 2018, **49**, 290.
41 M. Freunek, M. Freunek and L. M. Reindl, *IEEE J. Photovolt.*, 2013, **3**, 59.
42 D. P. McMeekin, G. Sadoughi, W. Rehman, G. E. Eperon, M. Saliba, M. T. Hörantner, A. Haghighirad, N. Sakai, L. Korte, B. Rech, M. B. Johnston, L. M. Herz and H. J. Snaith, *Science*, 2016, **351**, 151.
43 S. J. Yoon, S. Draguta, J. S. Manser, O. Sharia, W. F. Schneider, M. Kuno and P. V. Kamat, *ACS Energy Lett.*, 2016, **1**, 290.
44 E. T. Hoke, D. J. Slotcavage, E. R. Dohner, A. R. Bowring, H. I. Karunadasa and M. D. McGehee, *Chem. Sci.*, 2015, **6**, 613.
45 T. Duong, H. K. Mulmudi, Y. Wu, X. Fu, H. Shen, J. Peng, N. Wu, H. T. Nguyen, D. Macdonald, M. Lockrey, T. P. White, K. Weber and K. Catchpole, *ACS Appl. Mater. Interfaces*, 2017, **9**, 26859.
46 A. Sadhanala, F. Deschler, T. H. Thomas, S. E. Dutton, K. C. Goedel, F. C. Hanusch, M. L. Lai, U. Steiner, T. Bein, P. Docampo, D. Cahen and R. H. Friend, *J. Phys. Chem. Lett.*, 2014, **5**, 2501.